Tuning the colossal magnetoresistance in $(Mn_{1-x}Mg_x)_3Si_2Te_6$ by engineering the gap and magnetic properties via doping and pressure

Chaoxin Huang,[1] Mengwu Huo,[1] Xing Huang,[1] Hui Liu,[1] Lisi Li,[1] Ziyou Zhang,[2] Zhiqiang Chen,[2] Yifeng Han,[3] Lan Chen,[1] Feixiang Liang,[1] Hongliang Dong,[2] Bing Shen,[1] Hualei Sun,[4,*] and Meng Wang[1,†]

[1]*Center for Neutron Science and Technology, Guangdong Provincial Key Laboratory of Magnetoelectric Physics and Devices, School of Physics, Sun Yat-Sen University, Guangzhou 510275, China*

[2]*Center for High Pressure Science and Technology Advanced Research, Shanghai 201203, China*

[3]*Center for Materials of the University, School of Molecular Sciences, Arizona State University, Tempe, Arizona 85287, USA*

[4]*School of Science, Sun Yat-Sen University, Shenzhen 518107, China*

(Received 11 September 2023; revised 13 March 2024; accepted 6 May 2024; published 21 May 2024)

The ferrimagnetic semiconductor $Mn_3Si_2Te_6$ keeps the records of colossal magnetoresistance (CMR) and angular magnetoresistance (AMR). Here we report tuning the electronic transport properties via doping and pressure in $(Mn_{1-x}Mg_x)_3Si_2Te_6$. As the substitution of nonmagnetic Mg^{2+} for magnetic Mn^{2+}, ferrimagnetic transition temperature T_C gradually decreases, while the resistivity increases significantly. At the same time, the CMR and AMR are both enhanced for the low-doping compositions (e.g., $x = 0.1$ and 0.2), which can be attributed to the doping-induced broadening of the band gap and a larger variation range of the resistivity when undergoing a metal-insulator transition by applying a magnetic field along the c axis. On the contrary, T_C rises with increasing pressure due to the enhancement of the magnetic exchange interactions until a structural transition occurs at ∼13 GPa. Meanwhile, the activation gap is lowered under pressure and the magnetoresistance is decreased dramatically above 6 GPa where the gap is closed. At 20 and 26 GPa, weak drops in resistance indicating a superconducting transition at ∼5 K are observed. The results reveal that doping and pressure are effective methods to tune the activation gap, and correspondingly, the CMR and AMR in nodal-line semiconductors, providing an approach to investigate the magnetoresistance materials for novel spintronic devices.

DOI: 10.1103/PhysRevB.109.205145

I. INTRODUCTION

Since giant magnetoresistance was discovered in magnetic multilayers, the spin-charge coupling has been widely investigated for decades in a number of fields, including magnetic storage, magnetic sensor, magnetometer, and so on [1–6]. Colossal magnetoresistance (CMR) is more sensitive to a magnetic field than giant magnetoresistance whose variation in resistance can be close to 100%. CMR was first reported in doped manganese perovskite, where the double exchange mechanism and dynamic Jahn-Teller effect were demonstrated to play a key role [7–9]. Other mechanisms were suggested for the later discovered CMR materials, such as strong magnetic fluctuations in $EuCd_2P_2$ [10], magnetic polarons in $Ti_2Mn_2O_7$ [11,12] and $Eu_5In_2Sb_6$ [13], and spin-orbit coupling/spin-texture driven CMR in $EuTe_2$ and $EuMnSb_2$ [14–16]. Two-dimensional (2D) layered materials have higher spatial anisotropy, which is a fertile ground to explore new material systems with CMR and angular magnetoresistance (AMR) [16,17].

Indeed, the quasi-2D ferrimagnetic (FIM) semiconductor $Mn_3Si_2Te_6$ was found to exhibit the largest CMR and AMR, where the resistivity decreases by 10^7 as defined by $(\rho_H\text{-}\rho_0)/\rho_H$ for the $H \| c$ axis, but changes slightly in resistivity when H is along the ab plane [18–24]. It was suggested that the nodal-line degeneracy of $Mn_3Si_2Te_6$ can be controlled by spin orientation. When the applied field is along the c axis, spin-orbit coupling (SOC) between Mn and Te will result in band splitting and one of the bands will shift toward the Fermi level, leading to the closing of the electric gap and metal-insulator transition (MIT) [20]. Later, chiral orbital currents (COC) were suggested to circulate along the edges of $MnTe_6$ octahedra. In this scenario, the coupling between the spin of Mn^{2+} and the effective moments of the COC could reduce the electron scattering when a magnetic field was applied along the c axis [25]. However, single-crystal neutron diffraction and magnetization measurements reveal that the applied field along the c axis smoothly tilts the magnetic moment during the CMR occurs [19,20,26]. The activation gap may be a key gradient in the mechanism. Thus, further research to improve the magnitudes of the CMR and AMR and elucidate the mechanism is crucial to promote potential applications in the future.

Doping and pressure are considered effective methods to tune quantum transport properties in electronically correlated materials [27–32]. In this work, we report the successful synthesis of a series of $(Mn_{1-x}Mg_x)_3Si_2Te_6$ single crystals from $x = 0$ to 1.0 at 0.1 intervals and investigations of the evolutions of structure, magnetism, and electric transport properties with doping and pressure. We find the Mg doping can suppress the FIM, increase the resistivity by enlarging the activation

*sunhlei@mail.sysu.edu.cn
†wangmeng5@mail.sysu.edu.cn

gap, and enhance the CMR and AMR by about two orders of magnitude compared to the undoped compound. On the other hand, pressure induces the closure of the thermal activation gap at ∼7.0 GPa accompanied by the disappearance of the CMR, a structural transition at 14.6 GPa, and a superconducting transition at 5 K and 20 GPa. Our results reveal that the band gap can be widened or narrowed by doping or applying pressure, thus tuning the CMR and AMR to a required magnitude.

II. EXPERIMENTAL DETAILS

Single crystals of $(Mn_{1-x}Mg_x)_3Si_2Te_6$ $(0 \leqslant x \leqslant 1)$ were grown by the self-flux method and characterized by x-ray diffraction (XRD, Empyrean), energy dispersive x-ray spectroscopy (EDS, EVO Zeiss), Laue diffractometer (Photonic Science), and physical property measurement system (PPMS, Quantum Design). For partial samples with resistance exceeding the measuring range (e.g., data for $x = 0.1$ at low temperature and low field), an external voltammeter (Keithley) was employed while necessary.

High-pressure electrical transport measurements of $Mn_3Si_2Te_6$ single crystals were carried out using a miniature diamond anvil cell (DAC) made from a Be-Cu alloy on the PPMS. Diamond anvils with a 300 μm culet were used. The corresponding sample chamber with a 110 μm diameter was made in an insulating gasket achieved by a cubic boron nitride and epoxy mixture. KBr powders were employed as the pressure-transmitting medium, providing a quasihydrostatic environment. The pressure was calibrated by measuring the shift of the fluorescence wavelength of the ruby sphere, which was loaded in the sample chamber. The standard four-probe technique was adopted for these measurements.

The *in situ* high-pressure synchrotron powder XRD patterns were collected at 300 K with an x-ray wavelength of 0.6199 Å on the Shanghai Synchrotron Radiation Facility. A symmetric DAC with a pair of 300 μm diameter culet was used. The sample chamber was drilled by laser with a diameter of 120 μm. Daphne oil was used as the pressure-transmitting medium, and the pressure in the DAC was also calibrated by the shift of the fluorescence of the ruby sphere. The high-pressure XRD data were initially integrated using DIOPTAS [33] (with a CeO2 calibration) and fitted using the Pawley method in TOPAS-ACADEMIC V6 software [34].

III. RESULTS AND DISCUSSION

XRD measurements reveal that the crystal structure of $(Mn_{1-x}Mg_x)_3Si_2Te_6$ $(0 \leqslant x \leqslant 1)$ preserves the trigonal space group $P\bar{3}1c$. A small number of impurities of $MnTe_2$ can be identified in the XRD patterns of $x = 0$ and 0.4 compounds [35]. The lattice parameters are smoothly enlarged as the Mg doping. The nominal compositions are close to the EDS-determined compounds (Supplemental Material Fig. S1 [36]). We use the nominal x to indicate the composition of $(Mn_{1-x}Mg_x)_3Si_2Te_6$ throughout this paper.

Figure 1 shows the doping effects on magnetization and resistivity of $(Mn_{1-x}Mg_x)_3Si_2Te_6$. The temperature dependence of magnetization in Fig. 1(a) reveals a transition at

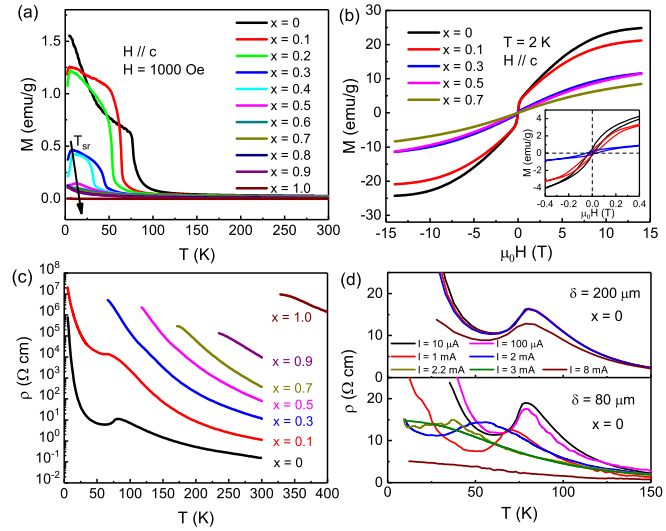

FIG. 1. (a) Temperature dependence of magnetization of $(Mn_{1-x}Mg_x)_3Si_2Te_6$ with the magnetic field parallel to the c axis and $H = 1000$ Oe. The arrow indicates the temperature T_{sr} of a spin reorientation. (b) Temperature dependence of magnetization of $(Mn_{1-x}Mg_x)_3Si_2Te_6$ at 2 K with an applied field parallel to the c axis from −14 to 14 T. The inset shows the hysteresis loops of the $x = 0$, 0.1, and 0.3 samples at low fields. (c) Temperature dependence of resistivity of $(Mn_{1-x}Mg_x)_3Si_2Te_6$. The resistivity of the $x = 1.0$ sample was measured from 328 to 400 K due to the large magnitude, which exceeded the measurement range at lower temperatures. (d) Temperature dependence of resistivity of $Mn_3Si_2Te_6$ with thicknesses of 200 and 80 μm measured with various currents.

∼78 K for $Mn_3Si_2Te_6$ that is consistent with the reported FIM order [37–40]. The FIM order is progressively suppressed with increasing doping until the disappearance for $x > 0.5$. In addition to the FIM transition, an abnormal decline on the magnetization curve can be observed at low temperatures for $0.1 \leqslant x \leqslant 0.5$, which could be ascribed to a spin reorientation transition due to a doping-induced magnetic dilution (Supplemental Material Fig. S2) [41]. The saturation magnetization decreases with increasing x [Fig. 1(b)]. The hysteresis loops resulting from the FIM can be observed in the low field range in both the undoped and doped samples [see inset in Fig. 1(b)].

The temperature dependence of the resistivity for different compositions is displayed in Fig. 1(c). Anomalies on the resistivity of $x = 0$ and 0.1 samples correspond to the T_Cs. When the x exceeds 0.1, the anomaly associated with T_C cannot be observed due to the limit of the measured resistance range. The values of the resistivity increase from 10^{-1} to 10^7 Ω cm at ∼300 K in the doping range of $0 \leqslant x \leqslant 1$. The resistivity for $Mg_3Si_2Te_6$ is too large to be measured below 328 K in our experimental setup [42]. We fit the resistivity above T_C using the polaron hopping model [40] $\rho(T) = AT\exp(E_a/k_BT)$, where E_a is the activation energy and k_B is the Bolzman constant. The results reveal linearly increased E_a from 83.5 to 408.6 meV with the Mg^{2+} doping (Fig. 5), revealing that the gap changes uniformly as doping, which may facilitate the electronic structure tuning in real applications. Figure 1(d) shows the resistivity measurements on $Mn_3Si_2Te_6$ single crystals with different currents and thicknesses. The T_C

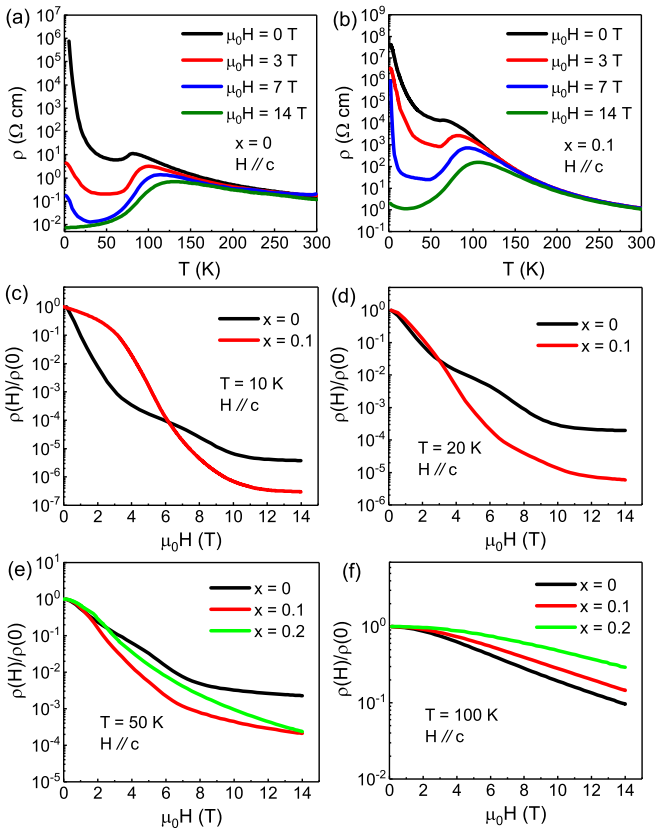

FIG. 2. (a) Resistivity as a function of temperature in different magnetic fields parallel to the c axis for the undoped sample and (b) for the $x = 0.1$ sample. (c) Field dependence of ρ_H/ρ_0 for the samples of $x = 0$ and 0.1 at 10 K, (d) 20 K, and for the samples of $x = 0$, 0.1, and 0.2 at (e) 50 K and (f) 100 K.

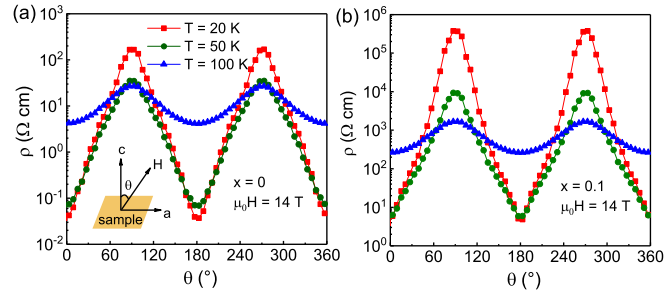

FIG. 3. (a) Angular dependence of resistivity for $Mn_3Si_2Te_6$ and (b) $(Mn_{0.9}Mg_{0.1})_3Si_2Te_6$ with $\mu_0 H = 14$ T at 20, 50, and 100 K. The inset in (a) shows the direction of the magnetic field, where θ is the angle between H and the c axis.

can be tuned by the magnitude of current for the single crystal with a thickness of $\sigma = 80$ μm, consistent with the previously proposed COC state [25]. However, the anomalies in resistivity for the $\sigma = 200$ μm sample are hardly changed until the current I is up to 8 mA. According to the discrepancy of the T_Cs for different currents and samples, the COC state does not depend on the current magnitude but the current density. The critical current density for the FIM state at 0 K is estimated to be 95 mA/mm^2 [Supplemental Material Fig. S1(d)].

To reveal the doping effect on the CMR, we show the temperature dependence of resistivity with magnetic fields parallel to the c axis for the undoped $x = 0$ and doped $x = 0.1$ compounds in Figs. 2(a) and 2(b). They all exhibit large CMR below the T_C. Similar measurements on the $x = 0.2$, 0.3, 0.5, and 0.7 compositions are shown in the Supplemental Material Fig. S3. At 5 K, the resistivity of $Mn_3Si_2Te_6$ drastically decreases by about eight orders of magnitude from 10^6 Ωcm at zero field to 10^{-2} Ω cm at $\mu_0 H = 14$ T. The change is smaller for $(Mn_{0.9}Mg_{0.1})_3Si_2Te_6$ at 5 K. However, over a wider temperature range from 10 K to the T_C, the drop of resistivity for the doped $x = 0.1$ compound under high magnetic fields is larger. To compare the CMR as doping quantitatively, we plot $\rho(H)/\rho(0)$ as a function of the magnetic field at 10, 20, and 50 K below the T_C, and 100 K above the T_C in Figs. 2(c) to 2(f). Due to the limitation of the measured resistivity range, the data of the $x = 0.2$ compound at 10 and 20 K are not shown in Figs. 2(c) and 2(d). The change of the magnitude of $\rho(H)/\rho(0)$ for the doped $x = 0.1$ sample is about two orders larger than that of the undoped $x = 0$ sample below T_C at 14 T. The magnitudes of $\rho(H)/\rho(0)$ reverse below 6.0 T at 10 K, 2.8 T at 20 K, and 1.8 T at 50 K, respectively. The CMR effect becomes much weaker above T_C as shown in Fig. 2(f). Thermal fluctuations, SOC, and the thermal activation gap are three ingredients that govern the CMR in $(Mn_{1-x}Mg_x)_3Si_2Te_6$. Increasing the temperature below T_C and strengthening the SOC will promote the conductance of electrons as expected. Our results demonstrate that substituting Mn^{2+} by nonmagnetic Mg^{2+} will enlarge the thermal activation gap, enhancing the CMR in this system.

Figure 3 shows a comparison of the colossal AMR for the undoped ($x = 0$) and doped ($x = 0.1$) compounds at 20 and 50 K below T_C and 100 K above T_C. The AMR exhibits a two-fold rotational symmetry. The resistivity as a function of the angle of the magnetic field to the c axis evolves close to linearly, consistent with the scenario that the spins of Mn^{2+} couple with the moments of the COC along the edges of the $MnTe_6$ octahedra [25]. Upon 10% Mg doping, the thermal activation gap is enlarged and the magnitude of the AMR in $(Mn_{0.9}Mg_{0.1})_3Si_2Te_6$ is enhanced an order at the same measurement conditions. Nonetheless, it is expected that the AMR will be enhanced in a wider doping range and at lower temperatures [20].

Pressure can effectively tune the structure, electronic transport, and magnetism of layered structural materials [29,31,43]. Figure 4(a) displays the high-pressure XRD patterns of $Mn_3Si_2Te_6$ up to 24.2 GPa. A clear structural transition is identified between 13.2 and 14.6 GPa, consistent with the reported Raman spectroscopy measurements [44]. The XRD patterns above 14.6 GPa are consistent with the space group $C2/c$ with a monoclinic structure where the lattice constants $a = 5.682$, $b = 4.080$, $c = 11.559$ Å, and $\beta = 97.88°$ at 14.6 GPa. The lattice parameters as a function of pressure can be deduced from the XRD patterns (Supplemental Material Fig. S4). However, the accurate atomic positions cannot be determined due to the limited reflection peaks.

Under pressure, the resistance measurements reveal a semiconducting to metallic transition [Fig. 4(b)]. Below the pressure of the structural transition, the T_C can be identified as a hump in resistance, yielding a linearly increased T_C from

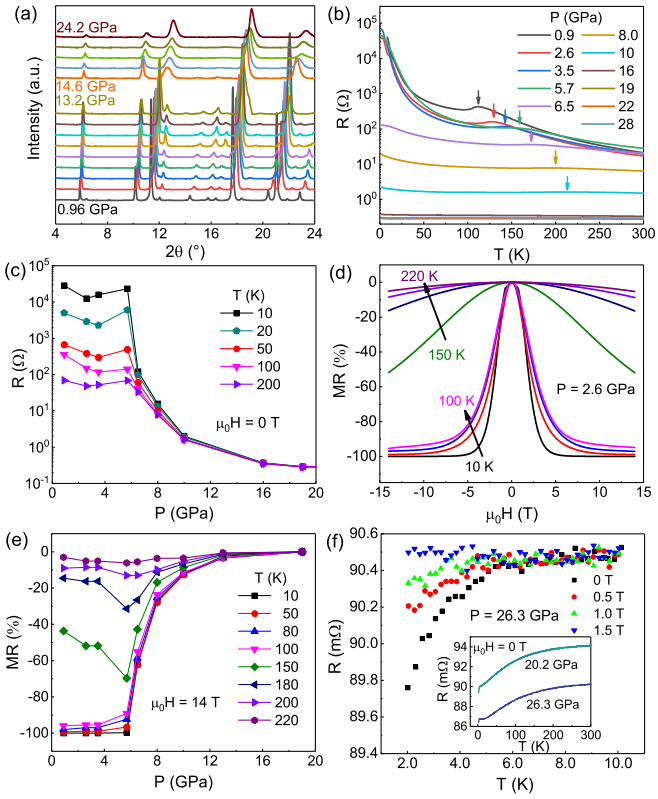

FIG. 4. (a) XRD patterns of $Mn_3Si_2Te_6$ under pressures from 0.96 to 24.2 GPa. A structural transition occurs between 13.2 and 14.6 GPa. (b) Temperature dependence of resistance of $Mn_3Si_2Te_6$ at various pressures up to 28 GPa. The Curie transition temperatures T_Cs under pressure are determined from the humps on resistance marked with the arrows. (c) Pressure dependencies of the resistance with $\mu_0 H = 0$ T and (e) the MR with $\mu_0 H = 14$ T at various temperatures. (d) MR defined by $(\rho_H\text{-}\rho_0)/\rho_0 \times 100\%$ at various temperatures at 2.6 GPa. (f) Resistance measurements below 10 K at 26.3 GPa and various magnetic fields. The inset shows the date from 2 to 300 K at 20.2 and 26.3 GPa with zero magnetic field. The drops of resistance at ~5 K and the behavior under magnetic fields indicate pressure-induced superconductivity.

~78 K at ambient pressure to ~214 K at 10 GPa. The thermal activation gap decreases with increasing pressure until closing at around 7 GPa. The activation gaps fitted by the polaron hopping model and the T_Cs of $Mn_3Si_2Te_6$ under pressure are presented in Fig. 5. The resistance measured at various pressures and temperatures also shows an abrupt drop at ~6 GPa [Fig. 4(c)]. Figure 4(d) shows typical magnetoresistance (MR defined as $(\rho_H\text{-}\rho_0)/\rho_0 \times 100\%$) measurements at 2.6 GPa and different temperatures (for more pressures, see Supplemental Material Fig. S5). The MR shows an abrupt change across $T_C = 127$ K at 2.6 GPa [Fig. 4(d)] and a sharp drop at ~6 GPa [Fig. 4(e)], revealing that the SOC and thermal activation gap are the dominating ingredients that govern the MR as elevated temperature and pressure, respectively.

The resistance of $Mn_3Si_2Te_6$ at 20.2 and 26.3 GPa are shown in Fig. 4(f) to investigate the electronic property of the monoclinic structure. Weak drops can be observed below 5 K on resistance. By applying a magnetic field up to 1.5 T, the resistance at 26.3 GPa below 5 K is enhanced obviously

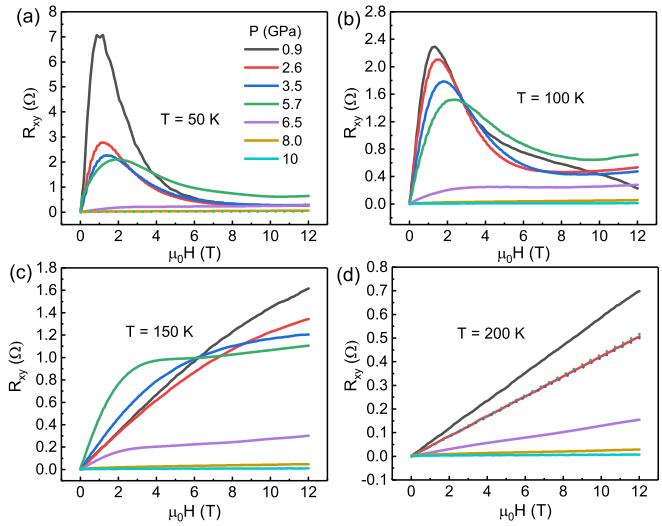

FIG. 5. (a) Hall resistance as a function of the magnetic field measured under different pressures at 50 K, (b) 100 K, (c) 150 K, and (d) 200 K. The pressures of the curves with different colors are labeled in (a).

and the drop is finally suppressed, indicating a superconducting transition. We note that it is common for Te-contained compounds showing superconductivity under pressure, such as WTe_2 [45,46], $CrSiTe_3$ [32], and $EuTe_2$ [30,47], where the electrons of Te play a dominating role in superconductivity.

FIM will result in an anomalous Hall effect. To double check the pressure-enhanced T_C of $Mn_3Si_2Te_6$, we show the Hall resistance in the pressure range of 0.9–10 GPa at different temperatures in Fig. 5. On the one hand, pressure will decrease the Hall effect due to the increased carrier density, which can be reflected in the Hall resistance in Figs. 5(a) to 5(c). On the other hand, pressure also enhances the FIM ordering

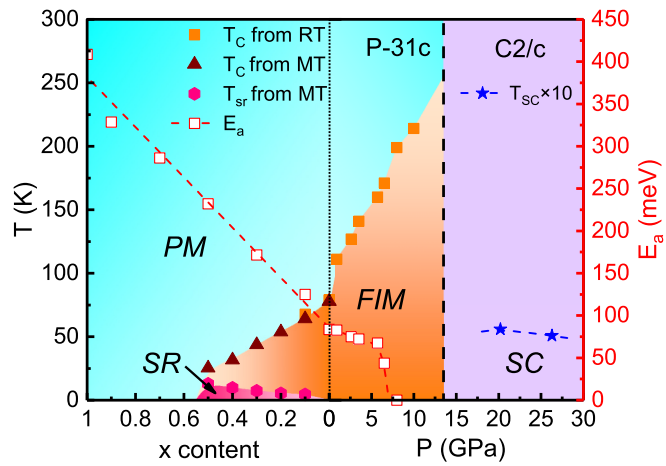

FIG. 6. A phase diagram of $(Mn_{1-x}Mg_x)_3Si_2Te_6$ aganist doping and pressure. The paramagnetic (PM), ferrimagnetic (FIM), spin reorientation (SR), and superconducting (SC) regions are determined by the resistance and magnetic measurements. Transition temperatures T_{SC}s of the possible superconductivity are magnified ten times for visualization. The thermal activation gaps, E_as, are fitted from the resistance.

temperature of $Mn_3Si_2Te_6$. The anomalous Hall resistance can be observed at 5.7 GPa and 150 K in Fig. 5(c), revealing the T_C has been increased and consistent with Fig. 4(b).

A comprehensive phase diagram combining the electronic, magnetic, and structural measurements as functions of doping and pressure is shown in Fig. 6. The T_C of the FIM transition decreases as doping but increases as applying pressure. The evolution of the thermal activation gap E_a reverses, changing from 408.6 meV in $Mg_3Si_2Te_6$ to 83.5 meV in $Mn_3Si_2Te_6$ at ambient pressure and closing at 7 GPa. The magnetoresistance decreases dramatically as the E_a closes, revealing that the CMR of $Mn_3Si_2Te_6$ is directly coupled with E_a. The presence of magnetoresistance requires SOC that is comparable with the electronic gap. In $(Mn_{1-x}Mg_x)_3Si_2Te_6$, the spins of Mn^{2+} possibly couple with the moments of the COC of the $MnTe_6$ octahedra. Superconductivity with a transition temperature of 5 K may exist in the monoclinic structure under pressures above 20 GPa.

IV. SUMMARY

In conclusion, we systematically studied the CMR, AMR, FIM, and structures of $(Mn_{1-x}Mg_x)_3Si_2Te_6$ as functions of doping and pressure. As Mn^{2+} is replaced by Mg^{2+} progressively, the FIM order is suppressed gradually until disappearing for $x > 0.5$. For the compositions with x between 0.1 and 0.5, a spin reorientation transition appears evidenced by a magnetic anomaly on magnetization at low temperatures. The thermal activation gap is enlarged linearly by the Mg doping. The CMR and AMR are both enhanced in the low-doped samples compared to the parent, which can be attributed to a doping-induced broadening of the band gap and a larger variation range of resistivity. On the contrary, T_C is enhanced with increasing pressure due to the enhanced magnetic exchange interactions until disappearing when undergoing a structural transition above 13.2 GPa. The gap closes and a MIT occurs at ~7 GPa, where the CMR is abruptly reduced. A possible superconducting transition at 5 K in the monoclinic phase under pressure is also observed. Our finding reveals that both doping and pressure are effective methods to change the band structure and magnetism, consequently enhancing the CMR and AMR in the FIM $(Mn_{1-x}Mg_x)_3Si_2Te_6$.

ACKNOWLEDGMENTS

The work at Sun Yat-Sen University was supported by the National Natural Science Foundation of China (Grants No. 12174454 and No. U2130101), the Guangdong Basic and Applied Basic Research Foundation (Grants No. 2021B1515120015 and No. 2022A1515010035), the Guangzhou Basic and Applied Basic Research Funds (Grant No. 2024A04J6417), the National Key Research and Development Program of China (Grants No. 2023YFA1406500 and No. 2023YFA1406002), and the Guangdong Provincial Key Laboratory of Magnetoelectric Physics and Devices (Grant No. 2022B1212010008). We also thank the BL15U1 station in Shanghai Synchrotron Radiation Facility (SSRF) for the help in characterizations.

[1] P. Grünberg, R. Schreiber, Y. Pang, M. B. Brodsky, and H. Sowers, Phys. Rev. Lett. **57**, 2442 (1986).
[2] M. N. Baibich, J. M. Broto, A. Fert, F. Nguyen Van Dau, F. Petroff, P. Etienne, G. Creuzet, A. Friederich, and J. Chazelas, Phys. Rev. Lett. **61**, 2472 (1988).
[3] J. Q. Xiao, J. S. Jiang, and C. L. Chien, Phys. Rev. Lett. **68**, 3749 (1992).
[4] S. M. Thompson, J. Phys. D **41**, 093001 (2008).
[5] I. Ennen, D. Kappe, T. Rempel, C. Glenske, and A. Hütten, Sensors **16**, 904 (2016).
[6] B. Dieny, J. Magn. Magn. Mater. **136**, 335 (1994).
[7] R. von Helmolt, J. Wecker, B. Holzapfel, L. Schultz, and K. Samwer, Phys. Rev. Lett. **71**, 2331 (1993).
[8] S. Jin, T. H. Tiefel, M. McCormack, R. Fastnacht, R. Ramesh, and L. Chen, Science **264**, 413 (1994).
[9] A. J. Millis, B. I. Shraiman, and R. Mueller, Phys. Rev. Lett. **77**, 175 (1996).
[10] Z.-C. Wang, J. D. Rogers, X. Yao, R. Nichols, K. Atay, B. Xu, J. Franklin, I. Sochnikov, P. J. Ryan, D. Haskel *et al.*, Adv. Mater. **33**, 2005755 (2021).
[11] Y. Shimakawa, Y. Kubo, and T. Manako, Nature (London) **379**, 53 (1996).
[12] P. Majumdar and P. Littlewood, Phys. Rev. Lett. **81**, 1314 (1998).
[13] P. Rosa, Y. Xu, M. Rahn, J. Souza, S. Kushwaha, L. Veiga, A. Bombardi, S. Thomas, M. Janoschek, E. Bauer *et al.*, npj Quantum Mater. **5**, 52 (2020).
[14] J. Yin, C. Wu, L. Li, J. Yu, H. Sun, B. Shen, B. A. Frandsen, D.-X. Yao, and M. Wang, Phys. Rev. Mater. **4**, 013405 (2020).
[15] H. Yang, Q. Liu, Z. Liao, L. Si, P. Jiang, X. Liu, Y. Guo, J. Yin, M. Wang, Z. Sheng *et al.*, Phys. Rev. B **104**, 214419 (2021).
[16] Z. Sun, A. Wang, H. Mu, H. Wang, Z. Wang, T. Wu, Z. Wang, X. Zhou, and X. Chen, npj Quantum Mater. **6**, 94 (2021).
[17] T. Ogasawara, K.-K. Huynh, T. Tahara, T. Kida, M. Hagiwara, D. Arčon, M. Kimata, S. Y. Matsushita, K. Nagata, and K. Tanigaki, Phys. Rev. B **103**, 125108 (2021).
[18] H. Vincent, D. Leroux, D. Bijaoui, R. Rimet, and C. Schlenker, J. Solid State Chem. **63**, 349 (1986).
[19] Y. Ni, H. Zhao, Y. Zhang, B. Hu, I. Kimchi, and G. Cao, Phys. Rev. B **103**, L161105 (2021).
[20] J. Seo, C. De, H. Ha, J. E. Lee, S. Park, J. Park, Y. Skourski, E. S. Choi, B. Kim, G. Y. Cho *et al.*, Nature (London) **599**, 576 (2021).
[21] G. Sala, J. Y. Y. Lin, A. M. Samarakoon, D. S. Parker, A. F. May, and M. B. Stone, Phys. Rev. B **105**, 214405 (2022).
[22] C. I. Kwon, K. Kim, S. Y. Kim, R. A. Susilo, B. Kang, K. Kim, D. Y. Kim, J. Kim, B. Kim, and J. S. Kim, Current Applied Physics **53**, 51 (2023).
[23] S. Djurdjic Mijin, A. Šolajić, J. Pešić, Y. Liu, C. Petrovic, M. Bockstedte, A. Bonanni, Z. V. Popović, and N. Lazarević, Phys. Rev. B **107**, 054309 (2023).
[24] S. W. Lovesey, Phys. Rev. B **107**, 224410 (2023).
[25] Y. Zhang, Y. Ni, H. Zhao, S. Hakani, F. Ye, L. DeLong, I. Kimchi, and G. Cao, Nature (London) **611**, 467 (2022).
[26] F. Ye, M. Matsuda, Z. Morgan, T. Sherline, Y. Ni, H. Zhao, and G. Cao, Phys. Rev. B **106**, L180402 (2022).
[27] Q. Zhang, J. Liu, H. Cao, A. Phelan, D. Graf, J. F. DiTusa, D. A. Tennant, and Z. Mao, NPG Asia Materials **14**, 22 (2022).

[28] Y. Zhang, L.-F. Lin, A. Moreo, and E. Dagotto, Phys. Rev. B **107**, 054430 (2023).
[29] H. Sun, L. Qiu, Y. Han, E. Yi, J. Li, M. Huo, C. Huang, H. Liu, M. Li, W. Wang *et al.*, Mater. Today Phys. **36**, 101188 (2023).
[30] H. Sun, L. Qiu, Y. Han, Y. Zhang, W. Wang, C. Huang, N. Liu, M. Huo, L. Li, H. Liu *et al.*, Commun. Phys. **6**, 40 (2023).
[31] H. Sun, C. Chen, Y. Hou, W. Wang, Y. Gong, M. Huo, L. Li, J. Yu, W. Cai, N. Liu *et al.*, Sci. China Phys. Mech. Astron. **64**, 118211 (2021).
[32] W. Cai, H. Sun, W. Xia, C. Wu, Y. Liu, H. Liu, Y. Gong, D.-X. Yao, Y. Guo, and M. Wang, Phys. Rev. B **102**, 144525 (2020).
[33] C. Prescher and V. B. Prakapenka, High Press. Res. **35**, 223 (2015).
[34] G. S. Pawley, J. Appl. Crystallogr. **14**, 357 (1981).
[35] Y. Xu, W. Li, C. Wang, Z. Chen, Y. Wu, X. Zhang, J. Li, S. Lin, Y. Chen, and Y. Pei, Journal of Materiomics **4**, 215 (2018).
[36] See Supplemental Material at http://link.aps.org/supplemental/10.1103/PhysRevB.109.205145 for details about the crystal structure, magnetization, resistivity under magnetic fields, and magnetoresistance.
[37] A. F. May, Y. Liu, S. Calder, D. S. Parker, T. Pandey, E. Cakmak, H. Cao, J. Yan, and M. A. McGuire, Phys. Rev. B **95**, 174440 (2017).
[38] Y. Liu, C. Petrovic *et al.*, Phys. Rev. B **98**, 064423 (2018).
[39] L. Martinez, H. Iturriaga, R. Olmos, L. Shao, Y. Liu, T. T. Mai, C. Petrovic, A. R. Hight Walker, and S. Singamaneni, Appl. Phys. Lett. **116**, 172404 (2020).
[40] Y. Liu, Z. Hu, M. Abeykoon, E. Stavitski, K. Attenkofer, E. D. Bauer, C. Petrovic *et al.*, Phys. Rev. B **103**, 245122 (2021).
[41] H. Liu, M. Huo, C. Huang, X. Huang, H. Sun, L. Chen, J. Xu, W. Yin, R. Li, and M. Wang, arXiv:2303.00597.
[42] C. Huang, B. Cheng, Y. Zhang, L. Jiang, L. Li, M. Huo, H. Liu, X. Huang, F. Liang, L. Chen *et al.*, Chin. Phys. B **32**, 037802 (2023).
[43] R. Olmos, P.-H. Chang, P. Mishra, R. R. Zope, T. Baruah, Y. Liu, C. Petrovic, and S. R. Singamaneni, J. Phys. Chem. C **127**, 10324 (2023).
[44] J. Wang, S. Wang, X. He, Y. Zhou, C. An, M. Zhang, Y. Zhou, Y. Han, X. Chen, J. Zhou *et al.*, Phys. Rev. B **106**, 045106 (2022).
[45] X.-C. Pan, X. Chen, H. Liu, Y. Feng, Z. Wei, Y. Zhou, Z. Chi, L. Pi, F. Yen, F. Song *et al.*, Nat. Commun. **6**, 7805 (2015).
[46] D. Kang, Y. Zhou, W. Yi, C. Yang, J. Guo, Y. Shi, S. Zhang, Z. Wang, C. Zhang, S. Jiang *et al.*, Nat. Commun. **6**, 7804 (2015).
[47] P. T. Yang, Z. Y. Liu, K. Y. Chen, X. L. Liu, X. Zhang, Z. H. Yu, H. Zhang, J. P. Sun, Y. Uwatoko, X. L. Dong *et al.*, Nat. Commun. **13**, 2975 (2022).